Improvement of Source Localization by Dynamical Systems Based Modeling (DSBM)

Christian Uhl*, Axel Hutt*, and Frithjof Kruggel*

Summary: Recently, we have proposed a new concept for analyzing EEG/MEG data (Uhl et al. 1998), which leads to a dynamical systems based modeling (DSBM) of neurophysiological data. We report the application of this approach to four different classes of simulated noisy data sets, to investigate the impact of DSBM-filtering on source localization. An improvement is demonstrated of up to above 50% of the distance between simulated and estimated dipole positions compared to principal component filtered and unfiltered data. On a noise level on which two underlying dipoles cannot be resolved from the unfiltered data, DSBM allows for an extraction of the two sources.

Key words: EEG/MEG; Dipole source modeling; Signal filter; Signal reconstruction; Dynamical systems.

Introduction

A major goal of the analysis of electro- and magnetencephalographic (EEG/MEG) data is the localization of brain activity during cognitive tasks. Source modeling in terms of fitting position, orientation and strength of dipole sources (Brenner et al. 1975; Scherg and von Cramon 1986; Mosher et al. 1992) has become a valuable tool for understanding brain functions.

Despite the success of dipole modeling, there are still open questions concerning dipole source localization, such as the definition of components (Rösler 1982) and corresponding time intervals for a basis of the fitting algorithm, and such as the choice of constraints to reduce the ambiguities of the inverse electromagnetic problem. Although the high temporal resolution of EEG/MEG measurements is one of the major advantages of this modality, conventional dipole modeling is not based on temporal aspects for an estimation of spatial parameters. In a recent paper (Uhl et al. 1998) we proposed a new concept for analyzing EEG/MEG data aiming at a reconstruction of the signal and its dynamics. The approach is based on a simultaneous fit of spatial and temporal parameters to given data sets, which we will call in following "dynamical systems based modeling" (DSBM). The reconstruction is achieved by minimizing a cost function considering signal representation - as it is done in principal component analysis (PCA) (Donchin and Heffley 1978) - and dynamic interactions. In our view, this may lead to more objective criteria for the characterization of EEG/MEG data sets, since interactions can be described and quantified.

In this paper we study the impact of DSBM as a reconstruction (or filter) technique with respect to source modeling. To investigate the performance, different data sets are simulated, different with respect to spatial and temporal characteristics as well as with respect to different noise levels. Since our approach can be viewed as an extension of PCA, source modeling results of PCA-filtered signals are compared with results of DSBM-reconstructed and unfiltered data sets.

Dynamical Systems Based Modeling (DSBM)

EEG/MEG signals represent electromagnetic potentials/fields measured on the scalp surface due to neuronal interactions in the human brain. The high-dimensional complex dynamical system on the neuronal level exhibits low-dimensional behavior on the level of measurements on the scalp surface, observed by correlation dimension studies (Babloyantz et al. 1985) as well as source modeling leading to low-dimensional dipole models. Therefore, one expects that the measurements $\mathbf{q}(t)$ (with the vector components representing the channels of the measurement) can be expressed as a combination of different field maps $\mathbf{u}_i$ weighted by factors x_i depending on time:

* Max-Planck-Institute of Cognitive Neuroscience, Leipzig, Germany.

Accepted for publication: October 24, 2000.

Correspondence and reprint requests should be addresssed to Axel Hutt, Max-Planck-Institute of Cognitive Neuroscience, Stephanstr.1a, D-04103 Leipzig, Germany.

Fax: ++49 341 9940 221

E-mail: hutt@cns.mpg.de

$$\mathbf{q}(t) = \sum_{i=1}^{n} x_i(t) \cdot \mathbf{u}_i. \tag{1}$$

Since information processing in the human brain is based on interactions of cell assemblies, the amplitudes $x_i(t)$ are not independent from each other, but reflect the interactions, which may be expressed in terms of differential equations:

$$\frac{\mathrm{d}}{\mathrm{d}t} x_i = f_i(\mathbf{x}). \tag{2}$$

A rigorous mathematical derivation for the emergence of low-dimensional dynamics in high-dimensional systems can be found in (Haken 1983, 1987) and applications of this concept to brain dynamics are reviewed in (Kelso 1995; Nunez 1995; Haken 1996; Kelso et al. 1998; Uhl 1998).

In a previous paper (Uhl et al. 1998) we outlined the link of EEG/MEG signals, brain functioning and dynamical systems, and presented an algorithm to dissociate the dynamically relevant subspace and the irrelevant subspace (noise) from given data sets. The interpretation of the fitted dynamical systems led to a new definition of components and we suggested that from this concept, more objective criteria for analyzing EEG/MEG data may evolve.

In this paper we present a slight modification of the algorithm presented in (Uhl et al. 1998) and discuss its application as a filter to improve source localization.

Algorithm

Based on the concept presented above, the goal of our approach is to decompose an event-related potential/field (ERP/F) signal $\mathbf{q}(t)$ into time-dependent amplitudes, $y_i(t)$, and spatial field distributions, $\mathbf{v}_i$, and to obtain a model in terms of differential equations of the underlying dynamics. An approximation of the spatio-temporal model may be obtained by minimizing a cost function, C, consisting of least-square-error functions of signal representation, C_S, and dynamics representation, C_D:

$$C = C_S + C_D \tag{3}$$

$$C_S = \frac{< \left(\mathbf{q}(t) - \sum_{i=1}^{n} y_i(t) \cdot \mathbf{v}_i \right)^2 >_t}{< (\mathbf{q}(t))^2 >_t} \tag{4}$$

$$C_D = \sum_i \frac{< (y_i - g_i(\mathbf{y}))^2 >_t}{< (y_i)^2 >_t} \tag{5}$$

with the brackets $< \ldots >_t$ denoting averaging over time.

Note that, compared to our cost function defined in Uhl et al. (1998), we slightly changed the definition: The results are similar, however the cost function (equation 3) is more transparently connected to the goal of decomposing the signal and modeling its amplitudes. To reduce possible ambiguities in the solution space, we constrain the amplitudes to

$$< y_i(t) \cdot y_j(t) >_t = \delta_{ij}. \tag{6}$$

After introduction of a set of biorthogonal modes $\mathbf{v}_i^+$ with $\mathbf{v}_i^+ \cdot \mathbf{v}_j = \delta_{ij}$, the unknown amplitudes can be written as a projection of the signal onto the biorthogonal modes:

$$y_i(t) = \mathbf{v}_i^+ \cdot \mathbf{q}(t) \tag{7}$$

Therefore, this projection procedure considers all channels, which has been shown to quantify spatially extended dynamics more reliably than single-channel methods (Lachaux 1997). Now, the cost function represents a function of spatial modes, $\mathbf{v}_i^+$, $\mathbf{v}_i$, and coefficients of the function g_i describing the dynamics:

$$C = C\left[\mathbf{v}_i^+, \mathbf{v}_i, g_i \right]. \tag{8}$$

Some of the parameters in the cost function can be eliminated analytically (Uhl et al. 1998), leading to a non-linear cost function depending on $\mathbf{v}_i^+$ only:

$$C = C\left[\mathbf{v}_i^+ \right]. \tag{9}$$

The constraint, (equation 6), can be considered for further reduction of parameter space (Uhl and Friedrich 1998).

The global minimum of the non-linear cost function has to be obtained by numerical methods, e.g., by a genetic algorithm (Holland 1987), and it represents the best choice to describe the signal and its dynamics with respect to the L_2 norm as defined in equations 4 and 5.

This approach represents an alternative to principal component analysis (PCA) (Donchin and Heffley 1978), which is also based on the minimization of a cost function, C_{PCA}, which is equivalent to the cost function C_S of our approach:

$$C_{\mathrm{PCA}} = \frac{< \left(\mathbf{q}(t) - \sum_{i=1}^{n} z_i(t) \cdot \mathbf{w}_i \right)^2 >_t}{< (\mathbf{q})^2 >_t} \tag{10}$$

Here, the minimum (for all n) with respect to $\mathbf{w}_i$ can be given analytically:

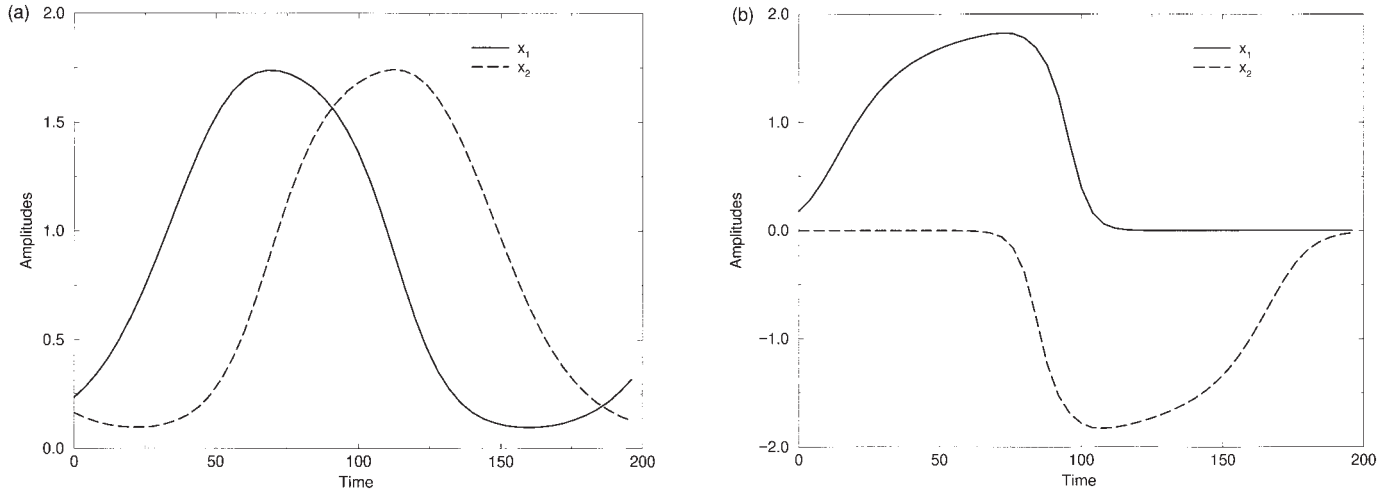

Figure 1. Amplitudes $x_1(t)$, $x_2(t)$, obtained from numerical integration of a) equations 27 and 28 (signals 1 and 2, overlapping amplitudes, same polarity) and b) equations 29 and 30 (signals 3 and 4, different polarity).

$$C\mathbf{w}_i = \lambda_i \mathbf{w}_i, \quad z_i(t) = \mathbf{w}_i \cdot \mathbf{q}(t) \tag{11}$$

with the eigenvalue λ_i of the correlation matrix $C_{ij} = < q_i q_j >_t$. The essential difference between PCA and our approach relies on the term C_D of the cost function. It deals with the interactions on which the signal is possibly based on. Mathematically, this represents a non-linear extension of PCA and leads to additional terms of higher order correlation tensors in equation 11.

Simulations

To evaluate DSBM as a filter technique and to investigate its effect on source localization, we simulated four different data sets $\mathbf{q}(t)$, consisting of the relevant signal $\mathbf{s}(t)$ and additive noise $\mathbf{n}(t)$:

$$\mathbf{q}(t) = \mathbf{s}(t) + \mathbf{n}(t) \tag{12}$$

Signals

The signals are modeled by dipoles $\mathbf{d}_1$ and $\mathbf{d}_2$ in a three-spheres head model. Its geometry is defined by radii of 94.8 mm, 88.2 mm and 83.8 mm with a conductivity relation of 1:0.0127:1. The center of the spheres is located at (x, y, z) = (7.4 mm; -2.9 mm; 56.0 mm) of the orthogonal coordinate system xyz with the posterior-anterior axis as the x-axis and the vertical axis z.

By solving the electromagnetic forward problem, potential field maps $\mathbf{u}_1(\mathbf{d}_1)$ and $\mathbf{u}_2(\mathbf{d}_2)$ on the scalp surface are obtained.

In our simulations, the time courses of the dipole strength are given by the amplitudes $x_1(t)$ and $0.4 \cdot x_2(t)$ with equal power of the amplitudes,

$$< x_1^2(t) >_t = < x_2^2(t) >_t = 1, \tag{13}$$

Thus we obtain

$$\mathbf{s}(t) = x_1(t) \cdot \mathbf{u}_1(\mathbf{d}_1) + 0.4 \cdot x_2(t) \cdot \mathbf{u}_2(\mathbf{d}_2) \tag{14}$$

To reflect different aspects of temporal and spatial characteristics, we introduce four classes of simulated signals using two sets of amplitudes $x_1(t)$, $x_2(t)$ and two sets of current dipoles leading to spatial field maps $\mathbf{u}_1(\mathbf{d}_1)$ and $\mathbf{u}_2(\mathbf{d}_2)$. The two sets of amplitudes show typical behaviour of dipole models (Mosher et al. 1992) in time and just differ in the relation of polarity to each other (figure 1a,b). Both the set with similar amplitudes and the set with different amplitudes are modeled by systems of differential equations, which are discussed in Appendix A.

The two sets of spatial field maps are also chosen to pairs of similar and different maps. Their underlying models are explained in Appendix A as well.

The resulting four classes of simulated data are shown in table I.

Noise

The noise term of the simulated data sets consists of three randomly chosen field maps $\mathbf{w}_i$ and random amplitudes $\eta_i(t)$:

$$\mathbf{n}(t) = n \cdot \sum_{i=1}^{3} \eta_i(t) \cdot \mathbf{w}_i \tag{15}$$

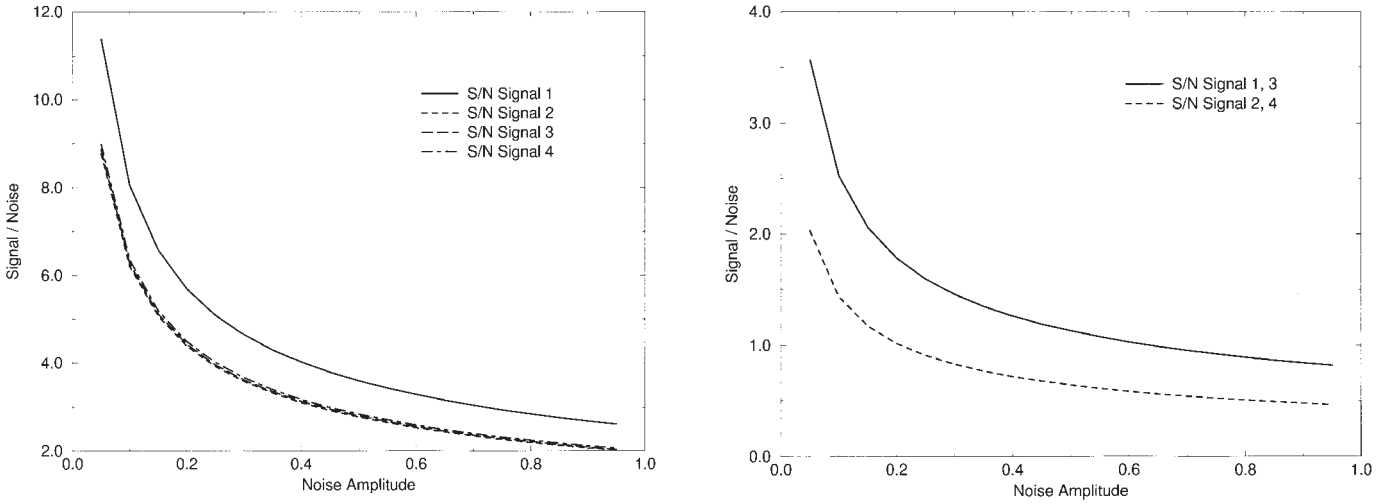

Figure 2. Signal-to-noise ratios (18) for the different classes of signals.

The factor n allows for tuning the signal-to-noise ratio. Each of field maps $\mathbf{w}_i$ are obtained by the forward solution of randomly chosen 16 radial dipoles from a pool of 210 positions equally distributed in the spherical head model. The random amplitudes are modeled by the formula

$$\eta_i(t) = N_i \sum_{j=1}^{10} \mathrm{e}^{-(t-\tau_i)^2/10}, \tag{16}$$

with a random-variable τ_i equally distributed in the time interval (0, 200). The factor N_i is introduced to normalize the amplitudes to $< \eta_i^2(t) >_t = 1$. Besides the presented temporal noise model, further noise models e.g., dealing with varying spatial distributions are also possible. Future investigations of dipole models by the presented method should deal with these noise models.

For each signal the noise intensity is varied by tuning the value n:

$$n = 0.05,\ 0.10,\ 0.15,\ldots,\ 0.90,\ 0.95 \tag{17}$$

Table I. Spatial and temporal characteristics of simulated signals 1-4.

amplitudes	Spatial field maps: similar	Spatial field maps: different
similar	Signal 1	Signal 2
different	Signal 3	Signal 4

The obtained signal-to-noise ratios (SNR) according to

$$S/N = \sqrt{\frac{\mathrm{pow}(\mathbf{s})}{\mathrm{pow}(\mathbf{n})}} \text{ with } \mathrm{pow}(\mathbf{a}(t)) =< \mathbf{a}^2(t) >_t \tag{18}$$

are shown in figure 2. We want to remark here, that the ratios are similar for signal classes 2-4 and smaller than signal class 1, since

$$\begin{aligned} \mathrm{pow}(\mathbf{s}) &= \mathbf{u}_1^2 + 0.4 < x_1 x_2 >_t \ \mathbf{u}_1 \cdot \mathbf{u}_2 + 0.4^2 \mathbf{u}_2^2 \\ &\cong \mathbf{u}_1^2 + 0.4 < x_1 x_2 >_t \ \mathbf{u}_1 \cdot \mathbf{u}_2 \end{aligned} \tag{19}$$

and $0.4 < x_1 x_2 >_t \mathbf{u}_1 . \mathbf{u}_2$ is small compared to $\mathbf{u}_1^2$ for signal classes 2-4.

Results

We compare results for the four simulations of the unfiltered signal $\mathbf{q}(t)$, the DSBM filtered signal $\mathbf{q}'_{\mathrm{DSBM}}(t)$,

$$\mathbf{q}'_{\mathrm{DSBM}}(t) = y_1(t) \cdot \mathbf{v}_1 + y_2(t) \cdot \mathbf{v}_2 \tag{20}$$

with the amplitudes $y_i(t)$ and spatial distributions $\mathbf{v}_i$ obtained by the algorithm described in a previous section, and PCA-filtered signals: a filtered signal based on one spatial distribution,

$$\mathbf{q}'_{PCA1}(t) = z_1(t) \cdot \mathbf{w}_1, \tag{21}$$

and a filtered signal based on two spatial distributions,

$$\mathbf{q}'_{PCA2}(t) = z_1(t) \cdot \mathbf{w}_1 + z_2(t) \cdot \mathbf{w}_2. \tag{22}$$

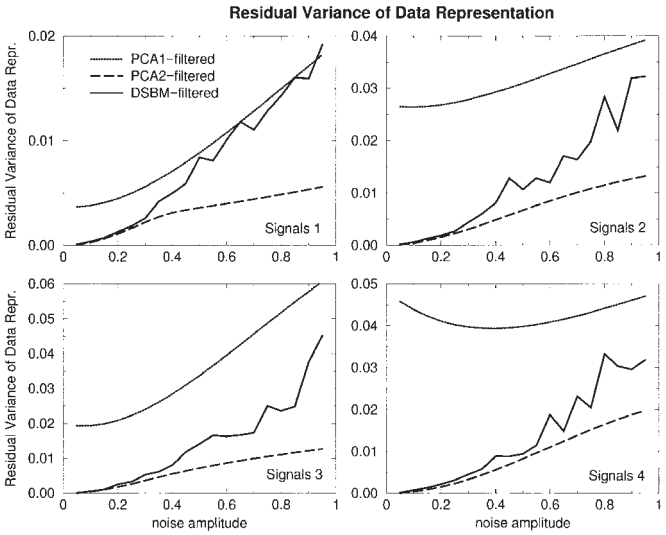

Figure 3. Residual variance of data representation (23) for the four classes of signals.

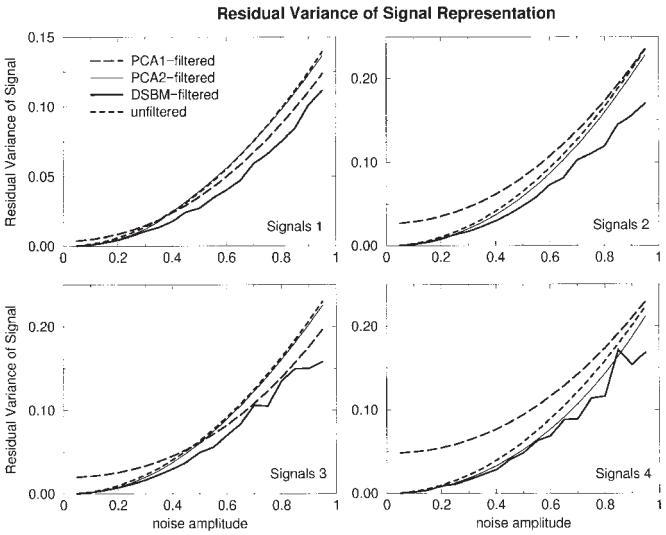

Figure 4. Residual variance of signal representation (24) for the four classes of signals.

Three measures will be utilized to compare the performance of the filters: data representation, signal representation and dipole position error as obtained by source modeling of the filtered signals. Note, that we distinguish between data, $\mathbf{q}(t)$, and signal, $\mathbf{s}(t)$, as defined in equation 12: we denote data as the underlying signal plus noise.

Residual variance of data representation

The residual variance of the data representation is given by

$$\frac{<\left(\mathbf{q}(t)-\mathbf{q}'(t)\right)^2>_t}{<\mathbf{q}^2(t)>_t} \qquad (23)$$

which is plotted for the four data classes in figure 3. Two features are observed: (1) The residual variance for the class 1 signals are considerably lower than the ones of the other signal classes. This is due to the similarities of the simulated spatial field maps as well as the simulated amplitudes. (2) With respect to this measure, the DSBM-filtered signal has a better performance than the PCA1-filtered data, since the two modes of the DSBM-filtered data capture more of the data than in the one-mode PCA-filtered case. It has an inferior performance than PCA2-filtered data, since both are based on a two-mode expansion, and PCA being solely based on an optimization of data representation.

Residual variance of signal representation

The goal of filtering ERP/F data sets is to separate signal from noise, and therefore the measure (equation 23) is not appropriate to quantify the filter quality. We chose the residual variance with respect to signal representation instead:

$$\frac{<\left(\mathbf{s}(t)-\mathbf{q}'(t)\right)^2>_t}{<\mathbf{s}^2(t)>_t} \qquad (24)$$

Results are plotted in figure 4 for the different signal classes. We included the unfiltered data set (dashed line) to emphasize the filtering effect. DSBM-filtered data show a lower residual variance than unfiltered and PCA-filtered data, which corresponds to a better noise separation by the DSBM method. PCA-filtering in contrast fails to separate signal from noise: PCA1-filtering reduces noise only for class 1 and 3 signals for a noise level above a certain threshold; below the threshold and for the signal classes 2 and 4, even the unfiltered data captures more of the signal than the PCA1-filtered data. PCA-filtering based on two-mode interactions only leads to small improvements in the case of type 4 signals, for all other types, PCA2-filtering is useless for signal reconstruction, since the unfiltered signal shows the same residual variance.

The failure of PCA-filtering with respect to separating signal from noise is due to the underlying optimization (compare equations 10 and 11) and resulting orthogonal modes $\mathbf{w}_i$: $\mathbf{w}_i \cdot \mathbf{w}_j = \delta_{ij}$. If the noisy part of the data is not orthogonal to the signal, $\mathbf{n}(t) \cdot \mathbf{s}(t) \neq 0$, it cannot be resolved by PCA. Since our approach does not assume an orthogonal decomposition, (i.e., $\mathbf{w}_i \cdot \mathbf{w}_j \neq \delta_{ij}$), we introduced a biorthogonal set of modes $\left(\text{i.e., } \mathbf{w}_i \cdot \mathbf{w}_j^+ = \delta_{ij}\right)$. The introduction of further degrees of freedom by the modes $\mathbf{w}_i^+$ is compensated by an additional cost function C_D, which can be regarded as a temporal constraint. Therefore, we are

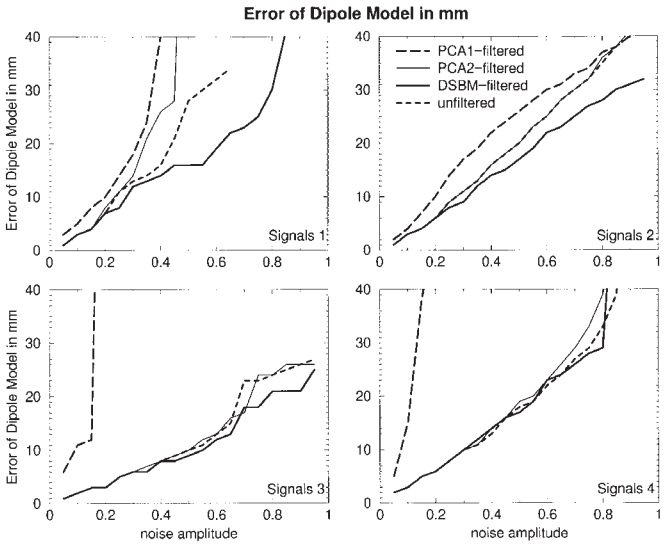

Figure 5. Absolute error of fitted dipole model (25) for the four classes of signals.

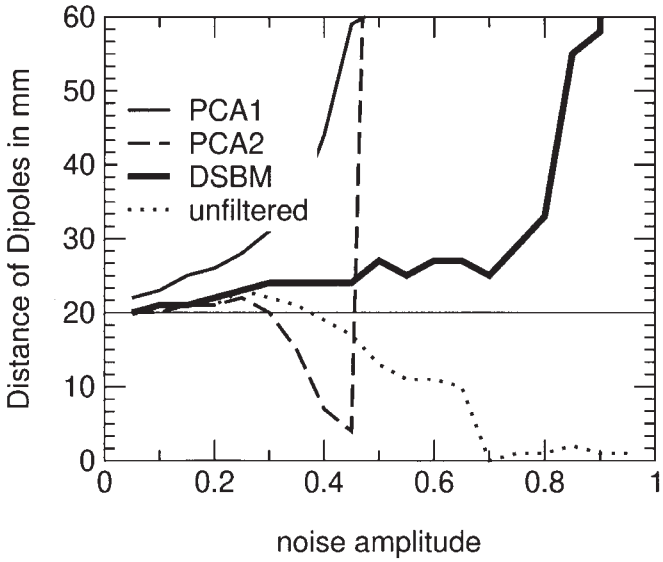

Figure 6. Distance of obtained dipole soultions (26) for class 1 signals.

able to partly separate signal from noise for the realistic case of data sets consisting of nonorthogonal signal and noise.

Comparison of dipole solutions

The impact of the improved signal-from-noise separation is investigated by a comparison of source models based on the inverse solution of the filtered and unfiltered data. The dipole fits are based on the spherical head model of the forward model (boundary element method) and were performed with ASA (A.N.T. Software b.v., Hengelo, Netherlands) by a non-linear Marquardt algorithm. As a starting point for the fitting algorithm we tested both the exact solution, $\mathbf{d}_1$ and $\mathbf{d}_2$, of the forward model and the solution of the dipole fit of the precedent noise level. The latter choice of starting points generally led to better solutions. The obtained dipole solutions are denoted as $\tilde{\mathbf{d}}_i$ and their distances to the exact positions represent a measure of the impact of DSBM-filtering:

$$\sqrt{\left(\mathbf{d}_1 - \tilde{\mathbf{d}}_1\right)^2} + \sqrt{\left(\mathbf{d}_2 - \tilde{\mathbf{d}}_2\right)^2} \qquad (25)$$

Errors are shown in figure 5 for the different signal classes and noise levels. Classes 3 and 4 show an extremely bad performance of the PCA1-filtered data sets, due to the spatial inhomogeneity of the underlying field maps (compare table I); results of PCA2-, DSBM- filtered and unfiltered data sets are similar, with an advantage for DSBM-filtered data of 3-5 mm (10-20%) for a noise level of $0.7 \leq n \leq 0.9$. For class 2 data, the DSBM-filtered signal yields the better improvement of dipole positions the higher the noise level is chosen: up to 10 mm (25%) in the case of noise level $n = 0.95$. Best results of the DSBM filter are obtained with class 1 data. PCA fails for noise levels $n \geq 0.4$ while DSBM improves dipole solutions by 12-17 mm (35-56 %) in the noise range of $0.5 \leq n \leq 0.65$. For even higher noise levels ($n > 0.65$) it is not possible to extract a two-dipole model from the unfiltered data. In the DSBM-filtered case the two-dipole model is still observable and yields only for high noise levels ($n > 0.9$) an error range above 40 mm.

To illustrate the problem of resolving the two dipoles in signal class 1, we plotted in figure 6 the distance,

$$\sqrt{\left(\tilde{\mathbf{d}}_1 - \tilde{\mathbf{d}}_2\right)^2}, \qquad (26)$$

of the two dipoles fitted to the unfiltered and the PCA- and DSBM-filtered data: For noise levels $n > 0.65$, the distance between the two dipole positions obtained from the unfiltered data vanishes, and thus they cannot be resolved anymore. The solutions of the PCA-filtered data sets show a distance of above 60 mm for $n \geq 0.5$. However, in the DSBM-filtered case, the distance is close to the exact value (20 mm, solid thick line) for $n < 0.8$ and increases for higher noise levels, while a two-dipole solution can be still obtained.

The success of DSBM-filtering especially in the case of class 1 signals is due to the spatial and temporal similarities of the two underlying components. In practical applications, if two adjacent cortical areas are activated during a cognitive task, both with the same polarity and a short latency between the components, DSBM-filtering may help to resolve the two components

and may lead to a source model which cannot be obtained by the unfiltered or PCA-filtered data.

Conclusions

We presented a new algorithm for modeling EEG/MEG data based on dynamical systems theory, which can be regarded as a filter technique. Its performance on separation of signal and noise from given measurements was studied by simulated data sets. We have shown that this filter technique is superior to principal component analysis and can improve source localization by more than 50% of the distance between simulated and estimated dipole position of the unfiltered or PCA-filtered data sets. For small signal-to-noise ratios the underlying dipoles still can be resolved by DSBM-filtered data in contrast to the failure of PCA-filtered and unfiltered data. Additionally, the method improves the separation of temporal activity of dipoles and the determination of relations between their amplitudes. When constraining the solution space by integrating realistic head models (Dale and Sereno 1993), the presented approach may lead to a deeper insight in spatio-temporal brain functioning.

Appendix

The characteristics of amplitudes and spatial field maps are implemented as follows:

Amplitudes

1. Two similar components with same polarity are obtained by numerical integration of

$$\frac{d}{dt}x_1 = 1/4 \cdot x_1 \cdot \left[1 - x_1 + x_2 \cdot (-4 + 4 \cdot x_1 + x_2)\right] \quad (27)$$

$$\frac{d}{dt}x_2 = -1/4 \cdot x_2 \cdot \left[1 - x_2 + x_1 \cdot (-4 + 4 \cdot x_2 + x_1)\right] \quad (28)$$

and initial conditions $x_1(t = 0) = x_2(t = 0) = 0.08$. Amplitudes are obtained after scaling by $1 / \sqrt{< x_i^2 >_t}$. They represent the amplitudes of the signal classes 1 and 2.
2. Two components with opposite polarity and smaller overlap are obtained by numerical integration of

$$\frac{d}{dt}x_1 = 1/4 \cdot x_1 \cdot \left[1 - 2 \cdot x_1 + x_1^2 + x_2 \cdot (x_2 - 4 \cdot x_1 + 4)\right] \quad (29)$$

$$\frac{d}{dt}x_2 = -1/4 \cdot x_2 \cdot \left[1 + 2 \cdot x_2 + x_2^2 + x_1 \cdot (x_1 - 4 \cdot x_2 - 4)\right]. \quad (30)$$

As initial conditions, $x_1(t = 0) = 0.05$, $x_2(t = 0) = -1 \times 10^{-6}$ are chosen, and again scaling of the amplitudes by $1 / \sqrt{< x_i^2 >_t}$ is applied. These amplitudes represent temporal dynamic of the simulated signal classes 3 and 4.

Spatial field maps

1. Similar field maps $\mathbf{u}_1$ and $\mathbf{u}_2$ are obtained by the forward solution of radial current dipoles with coordinates $\mathbf{d}_1$ = (-60, 20, 60) and $\mathbf{d}_2$ = (-60, 20, 80). The orientation vectors show just a small difference in the z-coordinates and thus lead to similar field maps. They are used for the signal classes 1 and 3.
2. Different field maps used in signal classes 2 and 4 are due to radial current dipoles with coordinates $\mathbf{d}_1$ = (-60, 20, 60) and $\mathbf{d}_2$ = (60, 20, 100). Here, the orientation of the dipoles differ much more than in the upper case, which leads to different spatial field maps. They contribute to the signal classes 2 and 4. In order to illustrate the method, the simple case of two radial current dipoles is chosen. The presented method is not restricted to this choice of number and orientation of dipoles.

References

Babloyantz, A., Nicolis, C. and Salazar, M. Evidence of chaotic dynamics of brain activity during the sleep cycle. Phys. Lett. A, 1985, 111: 152-156.

Brenner, D., Williamson, S.J. and Kaufman, L. Visually evoked magnetic fields of the human brain. Science, 1975, 190: 480-482.

Dale, A.M. and Sereno, M.I. Improved localization of cortical activity by combing EEG and MEG with MRI cortical surface reconstruction: a linear approach. Journal of Cognitive Neuroscience, 1993, 5(2): 162-176.

Donchin, E. and Heffley, E. Multivariate analysis of event-related potential data: a tutorial review. In: D. Otto (Ed.), Multidisciplinary perspectives in event-related potential research (EPA-600/9-77-043). Washington, DC: U.S. Government Printing Office, 1978.

Haken, H. Synergetics. An Introduction. Springer-Verlag, Berlin, 3rd edition, 1983.

Haken, H. Advanced Synergetics. Springer-Verlag, Berlin, 2nd edition, 1987.

Haken, H. Principles of Brain Functioning. Springer-Verlag, Berlin, 1996.

Holland, J.H. Adaption in Natural and Artificial Systems. Michigan University Press, Ann Arbor, 1987.

Kelso, J.A.S. Dynamic Patterns. The self-organization of brain and behavior. MIT Press, Cambridge, 1995.

Kelso, J.A.S., Fuchs, A., Lancaster, R., Holroyd, T., Cheyne, D. and Weinberg, H. Dynamic cortical activity in the human brain reveals motor equivalence. Nature, 1998, 392: 814-818.

Lachaux, J.-P., Pezard, L., Garnero, L., Pelte, C., Renault, B., Varela, F.V. and Martinerie, J. Spatial extension of brain activity fools the single-channel reconstruction of EEG dynamics. Human Brain Mapping, 1997, 5: 26-47.

Mosher, J.C., Lewis, P.S. and Leahy, R.M. Multiple dipole modeling and localization from spatio-temporal MEG data. IEEE Trans. BME, 1992, 39: 541-557.

Nunez, P.L. Experimental connections between EEG Data and the Global Wave Theory. In: P.L. Nunez (Ed.), Neocortical Dynamics and Human EEG Rhythms. Oxford University Press, Oxford, 1995.

Rösler, F. Hirnelektrische Korrelate Kognitiver Prozesse. Springer Verlag, Berlin, 1982.

Scherg, M. and von Cramon, D.Y. Evoked dipole source potentials of the human auditory cortex. Electroencephalogr. clin. Neurophysiol., 1986, 65: 344-360.

Uhl, C., Kruggel, F., Opitz, B. and von Cramon, D.Y. A new concept for EEG/MEG signal analysis: detection of interacting spatial modes. Human Brain Mapping, 1998, 6: 137-149.

Uhl, C. (Ed.), Analysis of Neurophysiological Brain-Functioning. Springer Verlag, Berlin, 1998.

Uhl, C. and Friedrich, R. Dynamical Systems Based Spatio-Temporal Modeling. In: C. Uhl (Ed.), Analysis of Neurophysiological Brain-Functioning.Springer Verlag, Berlin, 1998.